Thermal Characterization of Pockmarks Across Vestnesa and Svyatogor Ridges, Offshore Svalbard

M. Riedel[1] [ID], **H. Villinger[2]** [ID], **T. Freudenthal[3]**, **T. Pape[2,3]** [ID], **S. Bünz[4]** [ID], and **G. Bohrmann[2,3]**

[1]GEOMAR Helmholtz Centre for Ocean Research Kiel, Kiel, Germany, [2]Department of Geosciences, University of Bremen, Bremen, Germany, [3]MARUM-Center for Marine Environmental Sciences, University of Bremen, Bremen, Germany, [4]Centre for Arctic Gas Hydrate, Environment and Climate, Department of Geology, UiT The Arctic University of Norway, Tromsø, Norway

Abstract The Svalbard margin represents one of the northernmost gas hydrate provinces worldwide. Vestnesa Ridge (VR) and Svyatogor Ridge (SR) west of Svalbard are two prominent sediment drifts showing abundant pockmarks and sites of seismic chimney structures. Some of these sites at VR are associated with active gas venting and were the focus of drilling and coring with the seafloor-deployed MARUM-MeBo70 rig. Understanding the nature of fluid migration and gas hydrate distribution requires (among other parameters) knowledge of the thermal regime and in situ gas and pore fluid composition. In situ temperature data were obtained downhole at a reference site at VR defining a geothermal gradient of ~78 mK m^{-1} (heat flow ~95 mW m^{-2}). Additional heat probe data were obtained to describe the thermal regime of the pockmarks. The highest heat flow values were systematically seen within pockmark depressions and were uncorrelated to gas venting occurrences. Heat flow within pockmarks is typically ~20 mW m^{-2} higher than outside pockmarks. Using the downhole temperature data and gas compositions from drilling we model the regional base of the gas hydrate stability zone (BGHSZ). Thermal modeling including topographic effects suggest a BGHSZ up to 40 m deeper than estimated from seismic data. Uncertainties in sediment properties (velocity and thermal conductivity) are only partially explaining the mismatch. Capillary effects due to small sediment grain sizes may shift the free gas occurrence above the equilibrium BGHSZ. Changes in gas composition or pore fluid salinity at greater depth may also explain the discrepancy in observed and modeled BGHSZ.

1. Introduction

The Svalbard continental margin is one of the most studied Arctic gas hydrate provinces since it is a highly dynamic area with vigorous active free gas and aqueous fluid seepage, gas hydrate formation, and submarine slope failures (Hustoft et al., 2009; Posewang & Mienert, 1999; Vanneste et al., 2005; Vogt, Gardner, & Crane, 1999; Vorren et al., 1998). The margin has received substantial attention to study the shallow-water feather edge of the gas hydrate stability zone (GHSZ) where vast seafloor degassing was observed close to the expected outcrop of the base of GHSZ (BGHSZ) (Berndt et al., 2014; Ferré et al., 2020; Riedel et al., 2018; Wallmann et al., 2018; Westbrook et al., 2009). Gas hydrate research in deeper water (>600 m water depth) has focused on Vestnesa Ridge (e.g., Bünz et al., 2012) and Svyatogor Ridge (e.g., Johnson et al., 2015) west of Svalbard. These topographically prominent ridges are underlain by young oceanic crust that results in a highly variable heat flow regime (Figure 1, Crane et al., 1991). The northern sediment drift of the Vestnesa Ridge is separated by the Molloy Fracture Zone from the southern equivalent sediment drift of the Svyatogor Ridge (Johnson et al., 2015). These ridges consist of mostly fine-grained sediments, which are pierced by subvertical vent features (also referred to as acoustic chimneys) forming pockmarks at the seafloor (Goswami et al., 2015; Johnson et al., 2015; Petersen et al., 2010). These ridges have been a site of intense research in the past with numerous scientific expeditions studying the structure of the deep subsurface and properties of the sediments acquiring multibeam seafloor bathymetry, multichannel seismic (MCS) profiles, ocean-bottom seismometer, controlled-source electromagnetic, high-resolution subbottom profiler, and acoustic water column data, as well as sediment piston cores. During an initial study, Vogt et al. (1994) mapped the crest of Vestnesa Ridge showing abundant pockmarks, which was followed by sediment coring and some heat flow measurements (Vogt, Gardner, Crane, Sundvor, et al., 1999). Hustoft et al. (2009) discovered active seepage of free gas into the water column from one pockmark at the
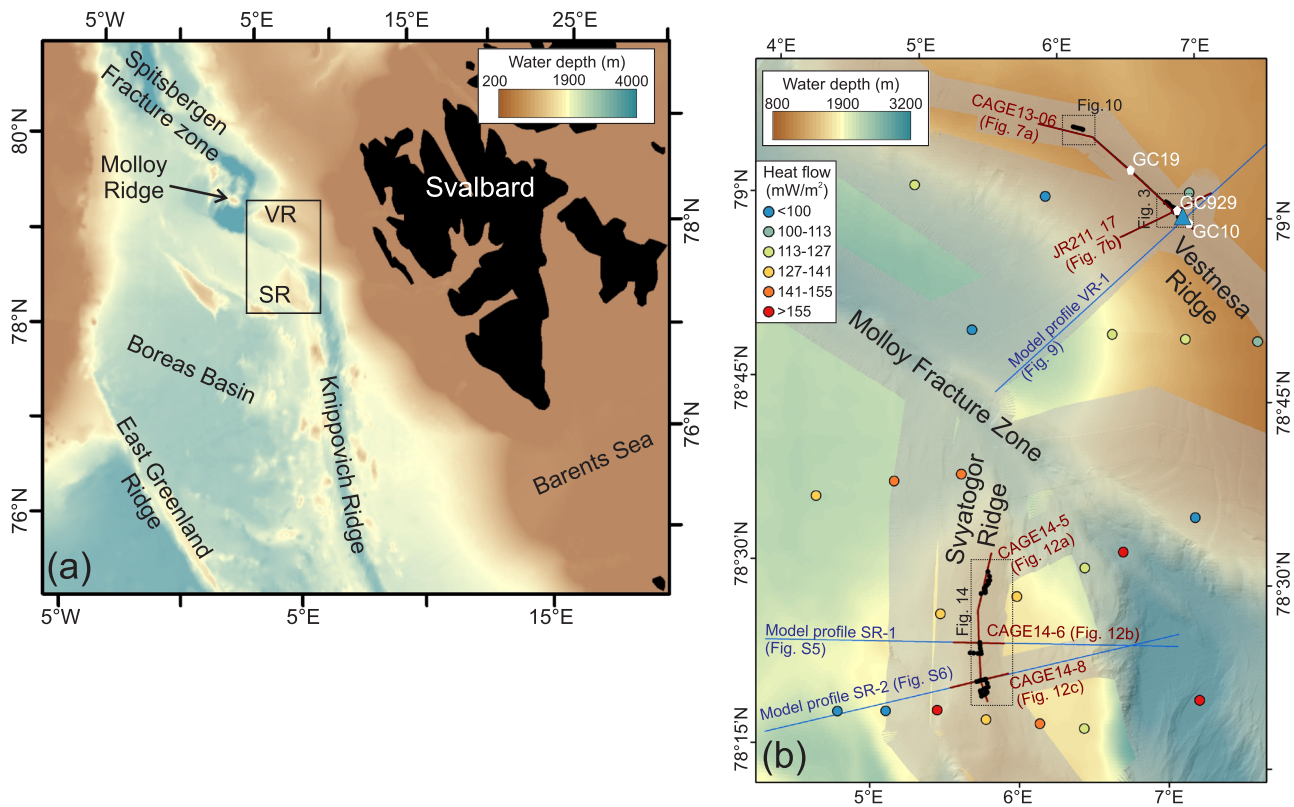
Figure 1. (a) Study region of the Vestnesa Ridge (VR) and Svyatogor Ridge (SR) at the Svalbard margin. (b) Detailed map of the ridges separated by the Molloy Fracture Zone. Detailed bathymetry is from expedition MSM57 (Bohrmann et al., 2017). In situ temperature measurements were made with MeBo70 at Vestnesa Ridge (Site GeoB21613-1: large blue triangle symbol with heat flow ~85 mW m^{-2}) and a total of 105 measurements with a shallow heat probe were made at VR and SR (black triangles, detailed results see maps in Figures 3 and 10). Regional heat flow values after Crane et al. (1991) are included. Three modeling transects (blue lines) were chosen to examine the effect of topography on heat flow (Figures 9, S5, and S6). Location of multichannel seismic data at VR and SR are shown as brown lines. Location of gravity cores (GC10 and GC19) from Plaza-Faverola et al. (2017) and GC929 from Smith et al. (2014) are shown in white along the profile CAGE13-06.

eastern edge of Vestnesa Ridge using hydro-acoustic imaging techniques. During repeat cruises in 2010 and 2012 it was found that active gas release is more widespread than previously assumed (Bünz et al., 2012; Smith et al., 2014). However, gas seepage seems to be mostly confined to the eastern portion of Vestnesa Ridge. The acoustically imaged gas flares extend in the water column to a depth of about 400 m below sea surface. This corresponds to the shallow limit of the theoretical GHSZ at Vestnesa Ridge (Smith et al., 2014), suggesting that gas bubbles are coated by a thin layer of solid hydrate that dissociates upon ascent of the gas to shallower water levels.

One of the open research questions at Vestnesa Ridge is on the structural control of gas seepage and pockmark formation. Bünz et al. (2012) and Plaza-Faverola et al. (2015) suggested that gas leakage is mostly facilitated by structural control and faults that extend to greater depths beneath the ridge. Gas can migrate laterally along permeable strata or along the BGHSZ. Through structural focusing and preferential pathways offered by abundant faults, the gas accumulates below the crest of the ridge. Structurally complex and heterogeneous fault systems were imaged with P-Cable 3-D seismic data at both, Vestnesa and Svyatogor Ridges showing abundant vertical conduits (chimneys) beneath the pockmarks (Bünz et al., 2012; Petersen et al., 2010; Plaza-Faverola et al., 2015). These piercement structures cut through the entire sediment column, linking several faults from greater depths and thereby connecting the free gas zone beneath the BGHSZ with the seafloor. The occurrence of seismic amplitude anomalies within the upper tens of meters inside these chimney features has previously been associated with the presence of massive gas hydrate, free gas pockets, or possibly carbonate concretions (Himmler et al., 2019; Panieri et al., 2014; Pape et al., 2020; Petersen et al., 2010; Plaza-Faverola et al., 2017; Smith et al., 2014).

Here, we report on the results of analyses using new thermal data obtained during drilling at Vestnesa Ridge with the MARUM-MeBo70 system (Freudenthal & Wefer, 2013) as part of the MARIA S. MERIAN expedition MSM57 (July/August 2016; Bohrmann et al., 2017). These downhole in situ temperature data are technically challenging to acquire and thus generally rare, especially in the Arctic environment. In situ temperature data acquired during the drilling are combined with a dedicated seafloor heat flow measurement campaign around the pockmarks along Vestnesa and Svyatogor Ridge. Temperature data, especially measured in situ at greater subseafloor depth, are an important component in understanding the gas hydrate system overall, especially offshore Svalbard, where the dynamic climate and tectonic history adds further complexity to the geologic setting (e.g., Himmler et al., 2019; Plaza-Faverola et al., 2015). Temperature profiles measured inside of pockmarks will reveal if any fluid flow is associated with gas seeps and will allow estimating fluid flow rates. During the same expedition MSM57, the MeBo70 was used to study the shallow (<400 m water depth) gas hydrate system off Svalbard (Riedel et al., 2018; Wallmann et al., 2018). Many of the technical details of using the temperature tool with MeBo70 were developed during these earlier studies and details are given in Riedel et al. (2018).

The objective of our study reported here is to characterize the heterogeneous distribution of heat flow across the pockmark chains, and to establish a reference temperature gradient in aid of regional gas hydrate related studies of the Vestnesa and Svyatogor Ridges. Defining such reference temperature gradient is important in understanding temperature anomalies linked to the vigorous gas flux observed at this margin (Smith et al., 2014), limiting uncertainties in predicting the total amount of gas hydrate occurrences along the margin, and building the base of additional analyses of sediment diagenesis (e.g., clay dehydration and liberation of fresh pore water) or other temperature-dependent processes such as hydrocarbon formation. The depth of the bottom simulating reflection (BSR) that marks the BGHSZ can principally be used as an isotherm allowing the estimation of surface heat flow variations (e.g., Plaza-Faverola et al., 2017). However, the laterally changing (but poorly constrained) heat flow trend along and across the ridge tied to the large-scale tectonic variation (Crane et al., 1991), as well as the variable geochemical composition of the advecting fluids and gas (Pape et al., 2020; Plaza-Faverola et al., 2017) allow a wide spectrum of possible scenarios and thus require ground-truthing of the thermal regime.

2. Data and Methods

2.1. Heat Probe

During expedition MSM57 we used a heat flow probe constructed in the classical violin bow design (Hyndman et al., 1979; Villinger et al., 2010). The probe consists of a strength member and 21 thermistors evenly distributed over the total length of a 6 m sensor tube, which also contains a heater wire for in situ thermal conductivity measurements (Lister, 1979). Measurements were conducted in a pogo-style fashion for operational efficiency, as initially described by Hyndman et al. (1979). The basic processing steps of raw heat flow measurements are outlined in Hyndman et al. (1979), Villinger and Davis (1986), and Villinger et al. (2010). Final heat flow values were calculated by using the in situ measured thermal conductivity where available. During the deployment of the heat probe, the tool's position was monitored with an acoustic transponder (USBL system POSIDONIA). The accuracy of defining the probe's position is on average 2% of the water depth. With an average water depth of ~1,200 m at both ridge crests, this results in an uncertainty of <25 m (~5% of the average diameter of the pockmarks). At each penetration, temperature-depth profiles were analyzed and thermal gradients were defined for the upper and lower portion of the profiles (details see Results). A table with all results is given in the supporting information. Assumed maximum penetration of the heat probe thermal string was 5.72 mbsf.

2.2. MeBo70 In Situ Temperature Measurements

A miniature temperature data logger (MTL; Pfender & Villinger, 2002) was utilized to measure bottom-hole temperatures in situ with the MeBo70. The original design of the MTL was modified so it fits into the pilot tube (details see Kopf et al., 2012; Bohrmann et al., 2017). The MTL is preprogramed in the onboard laboratory before it is mounted into the MeBo70 for deployment. Battery lifetime allows data recording at an interval of 3 s for a total of 48 hr. After completion of the drilling and recovery of the MeBo70 on deck, data are downloaded from the MTL as continuous ascii-data record including a time stamp and raw resistivity value. Temperature is obtained from these raw resistivity values based on calibration functions for the MTL

Table 1
Gas Molecular Composition (in mol-%) Used in Modeling of the Base of Gas Hydrate Stability

Gas	MeBo126, GeoB21613-1 (average for all depths)[a]	Feed-gas[b] (Smith et al., 2014)	GC19 (Plaza-Faverola et al., 2017)	GC10 (Plaza-Faverola et al., 2017)
	(mol-%)	n.i.	(vol.-%)	(vol.-%)
Methane	99.7406	99.0000	95.6000	99.5600
Ethane	0.2474	0.8400	2.0600	0.3400
Propane	0.0085	0.1600	2.3200	0.1000
i-Butane	0.0020	0.000		
n-Butane	0.0015	0.000		

Note. Concentrations of carbon dioxide in void gas samples from core GeoB21613-1 that was investigated in this study were below detection limit. n.i. = not indicated.
[a]A detailed list of depth-dependent concentrations is given in supporting information Table S3. [b]Assumed composition.

(defined in the laboratory at MARUM prior to the expedition) and depth is defined through matching of the MeBo70 tool performance records with the time stamps.

At regular downhole intervals, the MTL was inserted into the sediment at the bottom of the hole in front of the drill bit. This results in a typical frictional heating pulse that asymptotically decays over time to in situ temperatures (see Figure S1 for all time series of the deployments made with MeBo-70 during expedition MSM57). As the MTL is left in the sediments for up to 10 min, temperatures may reach in situ temperature of the formation by the end of the measurement period. However, as this may not always be the case, we estimated in situ values by plotting the measured temperatures as function of $1/t$ and linearly extrapolated to a value of $1/t = 0$, which is taken to be equivalent to the equilibrium temperature at $t = \infty$. Despite uncertainties due to drilling induced temperature disturbances, the accuracy of the geothermal gradient estimation is ~0.1 mK m^{-1} as discussed by Riedel et al. (2018).

2.3. Conversion of BSR Depth to Heat Flow

Seismic data across Vestnesa Ridge show a typical seismic reflection from the BGHSZ, referred to as BSR. As the BSR is in principle an isotherm (Grevemeyer & Villinger, 2001), it can be used to estimate regional thermal gradients and heat flow. Along two seismic lines that cross at Vestnesa Ridge and three lines across Svyatogor Ridge the depth of the BSR was determined in two-way traveltime and converted to depth using an average velocity of 1,680 m s^{-1} based on velocity data shown by Vanneste et al. (2005), Westbrook et al. (2008), Petersen et al. (2010), and Plaza-Faverola et al. (2017). The gas hydrate phase curve for assumed pore fluid salinity of seawater (3.4%) and different compositions of the gas listed in Table 1 based on the MeBo70 drilling results (Pape et al., 2020) and two cores by Plaza-Faverola et al. (2017) was determined with the CSMHYD program (Sloan, 1998). Gravity core station GC10 is close to the MeBo reference site.

2.4. Modeling the Topographic Effect

Using constraints of the bathymetry and general heat flow in the region (Crane et al., 1991), we model the effect of the seafloor topography and bottom water temperature variations depending on water depth on the local heat flow regime across the Vestnesa and Svyatogor Ridges. The general topography of the Vestnesa Ridge is an elongated crest in roughly NW-SE direction with a tight fold-axis in perpendicular orientation. We chose a modeling transect (location see Figure 1b) through the reference drill site (GeoB21613-1) and parallel to the MCS seismic line JR211_17 (Westbrook et al., 2009). The crest of Svyatogor Ridge is roughly N-S oriented. We completed two modeling transects (location see Figure 1b) parallel to the seismic lines CAGE14-6 around heat probe deployment sequence TL11 and CAGE14-8 around heat probe deployment sequence TL09. The modeling incorporates changing bottom water temperature as well as a depth-dependent thermal conductivity estimated from porosity measured at the reference drill site (GeoB21613-1). As thermal conductivity of pore water and methane hydrate exhibit very similar values (approximately 0.6 W m^{-1} K^{-1}; e.g., Yang et al., 2016), the derived depth-dependent thermal conductivity (Figure S4) is nearly independent on gas hydrate saturation variations across the study region. We used a 2-D numerical model of the cross section of the ridges to calculate the correction factors required to estimate
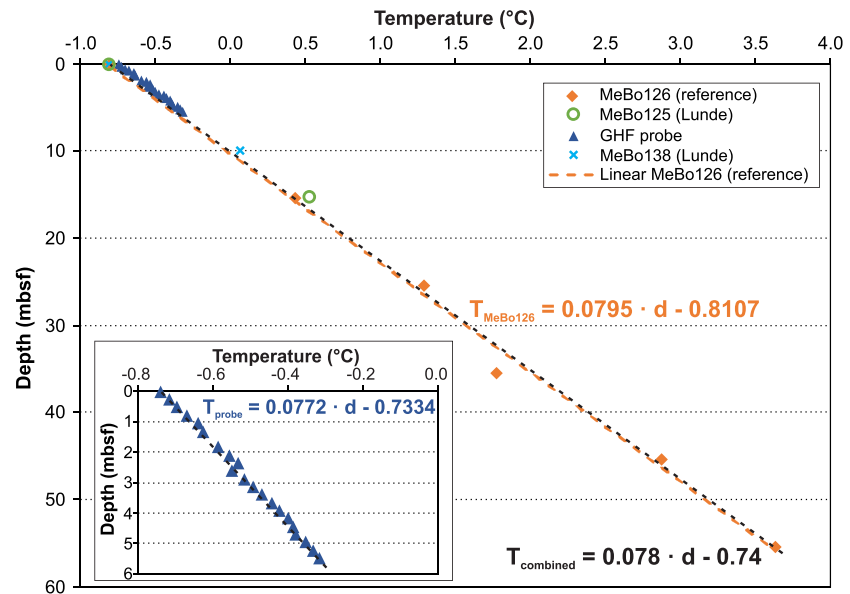
Figure 2. In situ temperature data shown as function of depth (d, in meter below seafloor, mbsf) from reference site GeoB21613-1 (MeBo126, orange symbols), and two deployments at Lunde pockmark (MeBo125: GeoB21610-1; MeBo138: GeoB21637-1). Inset shows heat probe data at the reference site (TL05-01, blue symbols). The data suggest a thermal gradient of ~79 mK m^{-1} which translates into a heat flow of ~95 mW m^{-2} using a thermal conductivity value of 1.2 W m^{-1} K^{-1}.

undisturbed heat flow. This model will allow estimating temperature at the BSR depths. All calculations were done with the Matlab® PDE Toolbox.

3. Results

3.1. Vestnesa Ridge

3.1.1. In Situ Temperature Measurements With MeBo70

Five temperature measurements with MeBo70 at the reference site combined with measurements of bottom water temperature (~−0.8°C) with the heat flow probe show a linear temperature increase with a gradient of 79.5 mK m^{-1} (Figure 2). In addition to the measurements at the reference site, two temperature deployments with MeBo70 were made inside the Lunde pockmark (Site GeoB21610-1 [MeBo125] and Site GeoB21637-1 [MeBo138]; Figure 3). Although these two individual temperature measurements inside Lunde did yield slightly higher temperatures at the same depths as suggested from the reference site (Figure 2 and Table 2), they do fall onto the same depth-trend as suggested by all combined data. A single deployment with the heat probe at the reference site yields a gradient of ~77 mK m^{-1} (inset Figure 2). Combining all these data yield an average background thermal gradient of 78 mK m^{-1}. Using an average in situ thermal conductivity of 1.2 Wm^{-1} K^{-1} results in a heat flow of ~95 mW m^{-2}. The individual temperature records from which in situ temperatures were determined of the seven deployments with MeBo70 are shown in the supporting information Figure S1.

3.1.2. Heat Probe Measurements

During six deployment sequences, a total of 69 stations were visited with the heat probe around the Lunde and Lomvi pockmarks as well as two additional pockmarks (named "A" and "B") further north along the crest of Vestnesa Ridge (Figure 3). All stations are grouped in locations falling clearly within a pockmark depression and those outside a depression (Table S1). Gas flares (indicator for active fluid flow) were observed only at Lunde and Lomvi pockmarks during repeat visits to this study area (2010, 2012, and during MSM57 in 2016; Bohrmann et al., 2017; Smith et al., 2014). Pockmarks "A" and "B" were not associated with active gas seepage during these visits.

In situ thermal conductivity was determined at 38 stations around the four pockmarks targeted with MeBo70 drilling (Figure 4 and supporting information Figure S2). Values are, when combining all stations and depth
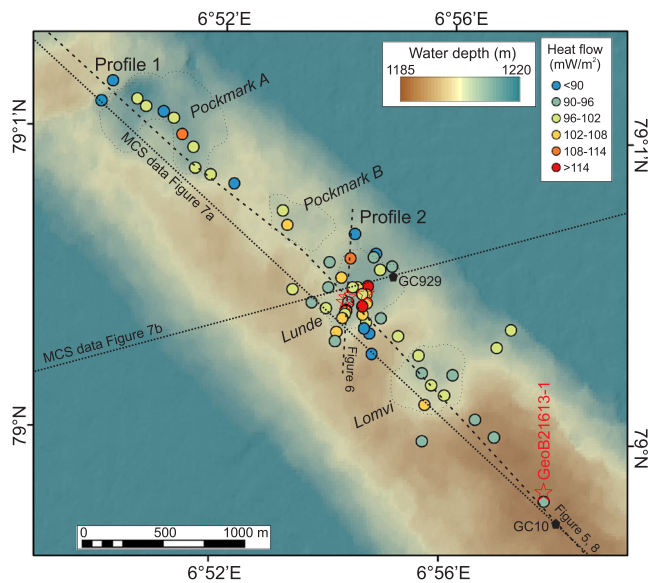
Figure 3. Map of heat flow values at the central Vestnesa Ridge with the pockmarks Lunde and Lomvi as well as unnamed Pockmarks A and B. Pockmark A is split into two small depressions, and Pockmark B is less pronounced in surface depression but is seen in PARASOUND data with the typical subseafloor acoustic masking. Drilling and coring stations with MeBo70 are shown as red stars. Southernmost station along Profile 1 is reference site GeoB21613-1, twinned with heat probe station TL05-01. The location of MCS data is shown by the dotted lines. Gravity core stations used to derive gas compositions are shown in black. Note that range in bathymetry values is optimized to show subtle variations in seafloor topography around the pockmark chain, not the regional scale water depth.

intervals penetrated, on average ~1.2 W m^{-1} K^{-1}. There is no systematic difference for stations inside or outside a pockmark depression. Therefore, this average value is used to estimate heat flow for all stations at Vestnesa Ridge, where no heat pulse was used. We also did not observe any change in bottom water temperature between stations other than the expected depth-dependent variations which we observe from the entire deployment record. At the depth range of the pockmarks visited across Vestnesa and Svyatogor Ridge, the temperature gradient in the water column measured just above the seafloor is only 0.0005°C m^{-1}. Two deployments of the heat probe at Stations 04-01 and 04-02 are compared (Figure 4) to show the difference of temperature and thermal conductivity for a station inside (04-02) and outside the Lunde pockmark (04-01).

The regional pattern of measured seafloor heat flow (Figure 3) at Vestnesa Ridge is that heat flow is systematically enhanced inside a pockmark depression. Measured heat flow outside a depression is generally lower than 95 mW m^{-2}, whereas heat flow values inside a pockmark are generally higher than 95 mW m^{-2} (with the exception of station TL03-07 at the Lomvi pockmark, Table S1). This is best visualized plotting heat flow values along the crest of Vestnesa Ridge (Profile 1; Figure 5) following the PARASOUND data, and across the Lunde pockmark (Figure 6) in an E-W orientation.

3.1.3. Seismic Structure of Vestnesa Ridge and BSR

The low frequency (<120 Hz) MCS data (Vanneste et al., 2005; Westbrook et al., 2009) show that the crest of the Vestnesa Ridge anticline is marked by numerous seafloor pockmarks linked to faults that penetrate to below the BGHSZ (Figure 7a). The BSR, marking the BGHSZ, is not always seen as an isolated reflection, but can rather

be identified only by the onset of a high reflectivity zone (Vanneste et al., 2005). This high reflectivity zone is only of limited lateral extent (~4 km) underneath the crest of Vestnesa Ridge and is the result of the presence of free gas enhancing the impedance contrast of gas-rich to gas-free sediments (Figure 7b). At several pockmarks, short segments (few tens of meters in length only) of high reflection amplitude are seen within the upper 20–30 m below seafloor (mbsf) (Panieri et al., 2017). Those amplitude anomalies can be the result of either high concentrations of gas hydrate, free gas pockets, or carbonate concretions. Drilling and coring at the Lunde pockmark during expedition MSM57 revealed that one such shallow bright amplitude spot resulted from the presence of carbonate concretions (Bohrmann et al., 2017; Himmler et al., 2019). The pockmarks themselves appear especially in the high frequency (~3.5 kHz) acoustic sub bottom profiler (PARASOUND) data as wipeout zones (Figure 8). Individual reflectors at the edge of the pockmarks (or blank zones) appear to be pulled down into the structure, often resulting in V-shaped reflection imagery, which in most cases is the result of edge diffractions.

Table 2
Estimated In Situ Temperatures Obtained With MeBo70 at Vestnesa Ridge

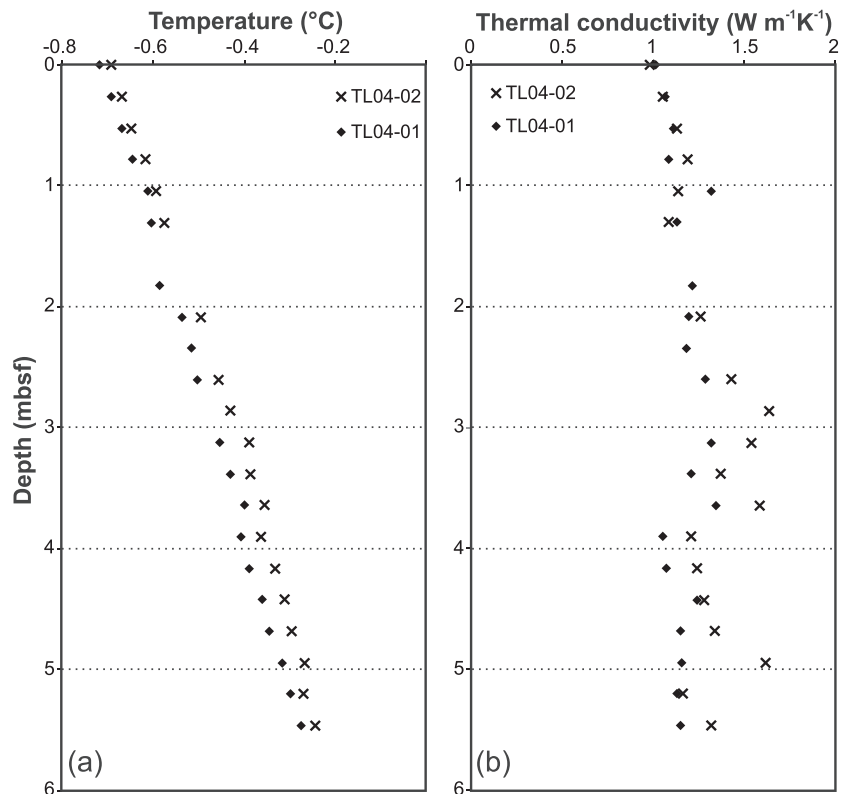| Site	Depth below seafloor (m)	Temperature (°C)
GeoB21613-1 (reference, MeBo126)	0	−0.801
	15.4	0.433
	25.4	1.290
	35.4	1.774
	45.4	2.871
	55.4	3.636
GeoB21610-1 (MeBo125)	0	−0.793
	15.4	0.531
GeoB21637-1 (MeBo138)	0	−0.810
	9.88	0.070

Figure 4. Example of variation of (a) temperature and (b) thermal conductivity with depth at a station inside (04-02) and outside (04-01) Lunde Pockmark. Thermal gradient at the station inside the pockmark is 106.7 and 95.1 mK m^{-1} outside the pockmark.

The MCS and PARASOUND data show a regular sedimentary system of seafloor parallel layers that can be traced across and along the crest of Vestnesa Ridge (Figure 8). Drilling and coring with MeBo70 at the reference site GeoB21613-1 penetrated the upper 62.5 mbsf with a core recovery of ~42%. Sediments are predominantly silty clay with some occurrence of coarser-grained lithology (with pebbles up to 5 cm in diameter) interpreted as ice-rafted debris (Panieri et al., 2017). The frequent occurrence of the pebble-sized ice-rafted debris is the reason for the overall poor core recovery. At this reference site, coring and subsequent analyses did not reveal any evidence within the uppermost 62 mbsf of the in situ presence of gas hydrate (e.g., no pore fluid freshening or cold-spot anomalies detectable with infrared imaging, Bohrmann et al., 2017; Pape et al., 2020).

3.1.4. Topographic Modeling at Vestnesa

Vestnesa Ridge has a pronounced topography and a relatively steep western flank with water depths increasing from ~1,200 m at the ridge crest to ~2,300 m along a 35 km distance (Figure 1). Using the topographic change along a profile across the ridge crest (nearly parallel to seismic line JR211_17; Figure 7b) and implementing estimates of depth-dependent porosity and thermal conductivity (Figure S4), steady-state conductive surface heat flow was predicted (Figure 9). The modeling is conducted using a background heat flow that reproduces the down hole measurements, which in our case is ~104 mW m^{-2}. Overall, seafloor topography results in a maximum 10% reduction of measured heat flow at the top of the ridge with respect to the undisturbed heat flow at depth. Including the 2-D topographic effect results in a temperature of ~11.9°C at the assumed depth of the base of gas hydrate stability (and BSR) at ~200 mbsf. Using instead a linear thermal gradient as defined from the MeBo70 data and surface heat probe deployment at the reference site predicts a temperature of ~15°C at the same depth of 200 mbsf.

3.2. Results From Northern Fault Crossing

Five measurements of heat flow were carried out at a sub region ~18 km northwest along the crest of the Vestnesa Ridge that showed prominent steps in seafloor which are linked to fault traces cutting the ridge
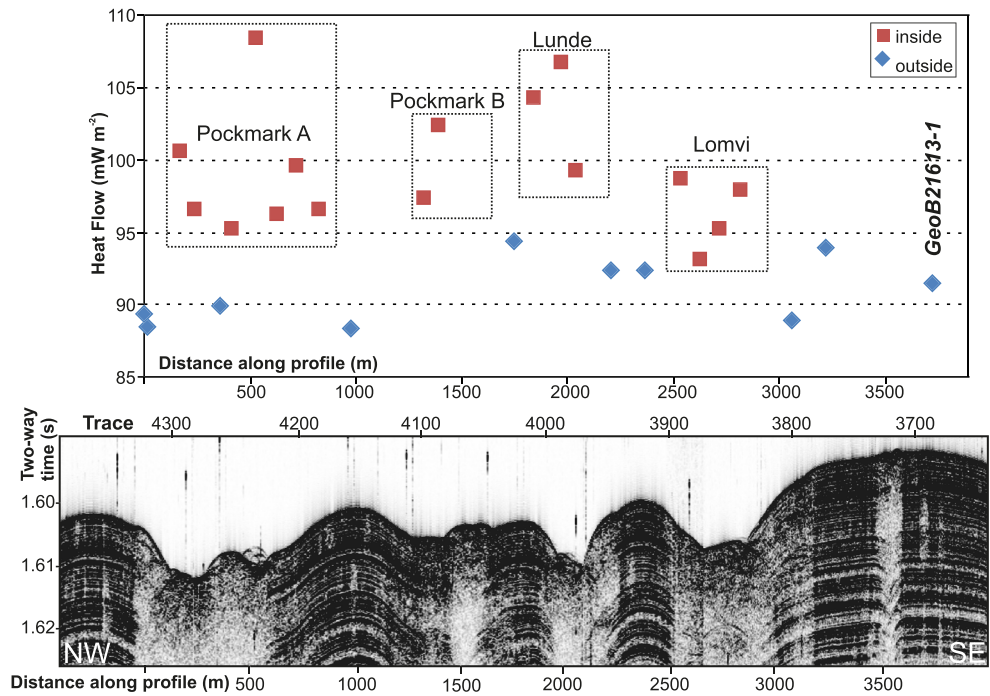
Figure 5. Heat flow values along chain of pockmarks projected onto a NW-SE trending PARASOUND profile (Profile 1, location see Figure 3, vertical exaggeration: 40). Values from stations inside a pockmark are shown as red squares, and values from outside a pockmark are shown as blue diamonds.

in a crest-perpendicular orientation (Figure 10). The fault traces are seen in the PARASOUND data as prominent V-shaped deflections of individual reflectors (Figure 11). The heat flow values of all five stations (ranging from 98–125 mW m^{-2}) are all higher than the background measured with the MeBo70 at Site GeoB21613-1 (~90 mW m^{-2}) and outside of the pockmarks Lunde and Lomvi (Figure 5).

3.3. Results From Svyatogor Ridge

3.3.1. Seismic Character of the Pockmarks and BSR

Chains of pockmarks across the Svyatogor Ridge were previously observed (Johnson et al., 2015). However, no active gas venting was seen anywhere during previous expeditions in 2014 and 2015 (Waghorn et al., 2018), as well as expedition MSM57 in 2016 (Bohrmann et al., 2017). Across Svyatogor Ridge, seismic data show a BSR (Figure 12) indicating existence of a gas hydrate system with free gas accumulating beneath the phase boundary (Johnson et al., 2015). The BSR is often only discernable as the upper truncation of bright amplitudes along dipping strata. The shallow (<50 mbsf) subsurface structures were imaged during expedition MSM57 with the PARASOUND system (Figure 13). Similar to the northern Vestnesa Ridge, the subbottom profiler data reveal mostly seafloor parallel sediment layering. Pockmarks, often acoustically transparent, show the typical V shape depressions.

3.3.2. Heat Probe Measurements

Heat flow around the pockmark chains were mapped with a total of 36 stations across three subregions of the Svyatogor Ridge (Figure 14). Only one station per pockmark clearly inside a depression was targeted to investigate if the same heat flow pattern seen north across Vestnesa Ridge also exists at Svyatogor Ridge. As
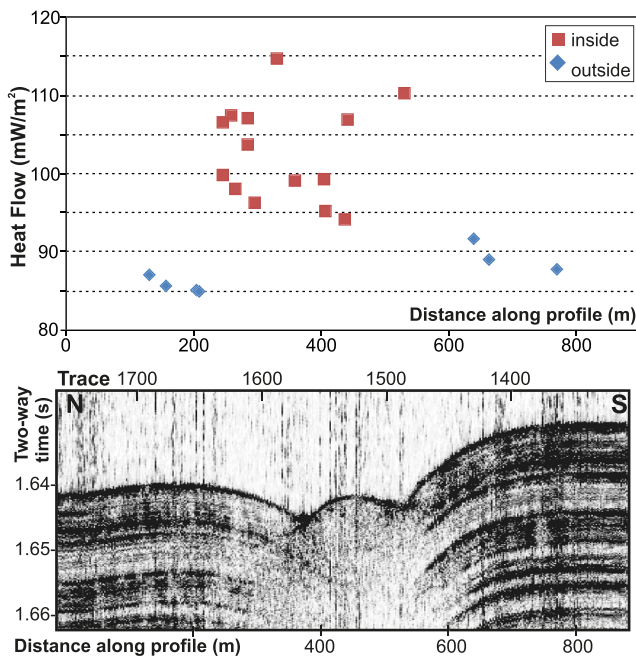

Figure 6. Heat flow values across Lunde pockmark projected onto a N-S-trending PARASOUND profile (profile 2, location see Figure 3, vertical exaggeration: 14). Values from stations inside the pockmark are shown as red squares, and values from outside the pockmark are shown as blue diamonds.
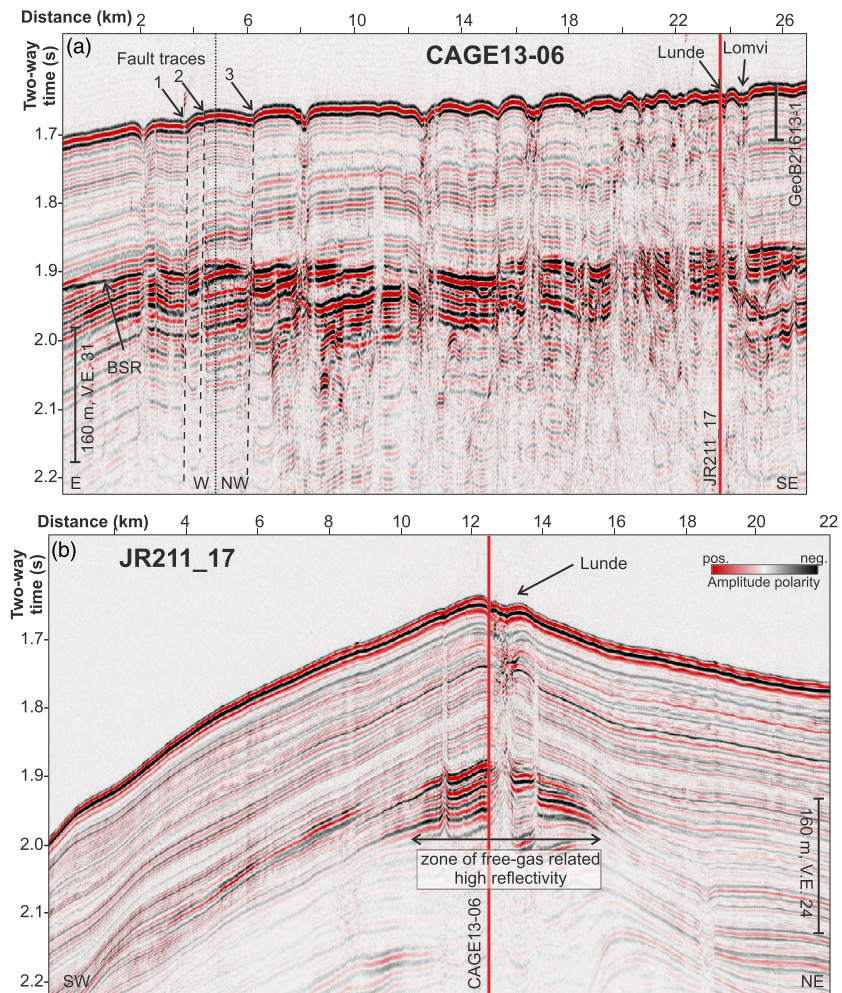
Figure 7. (a) Seismic line CAGE13-06 along the crest of Vestnesa Ridge. A bend in the line is indicated by the vertical dashed line (locations of line, see Figure 1). The regions of heat flow measurements are at the fault site and around the Lunde and Lomvi pockmarks. The MeBo70 drill site (GeoB21613-1) is seen at the SE end of the line with an ~62 m penetration (75 ms two-way time based on a velocity of 1,600 m/s). The area is characterized by numerous seismic blank zones that penetrate the entire sediment section from greater depth to seafloor. (b) Seismic line JR211_17 (Westbrook et al., 2009) across the crest of Vestnesa Ridge at Lunde pockmark demonstrating that the high reflectivity from free gas beneath the base of gas hydrate stability is focused around a 2–3 km short stretch beneath the crest only. Amplitude polarity is identical on both sections.

expected from the regional heat flow trend (Crane et al., 1991; Figure 1b), heat flow at Svyatogor Ridge is overall higher than at Vestnesa Ridge. The lowest heat flow estimated at Svyatogor Ridge was ~119 mW m^{-2} (Table S2) compared to ~85 mW m^{-2} at Vestnesa Ridge. Thermal conductivity at the sites of Svyatogor Ridge measured with the heat pulse appears overall slightly higher with an average value of 1.31 W mK^{-1} compared to sites of Vestnesa Ridge (which was 1.2 W mK^{-1}). There is no systematic difference in the depth trend of thermal conductivity for sites within or outside a pockmark. Therefore, the average value of 1.3 W mK^{-1} was used to estimate heat flow for those stations at Svyatogor Ridge where no heat pulse was used.

3.3.3. Topographic Model of Svyatogor Ridge
Similar to Vestnesa, the Svyatogor Ridge is an exposed topographic ridge with seafloor dropping significantly on both flanks. Along two profiles, parallel to existing seismic data (shown in Figures 12b and 12c) and across the deployment sequences TL09 and TL11, the topographic effect on the heat flow regime was investigated (Figures S5 and S6). Heat flow at both these transects across Svyatogor Ridge is reduced by ~10% underneath the ridge crest. Modeling was conducted with a depth-dependent seafloor temperature. We
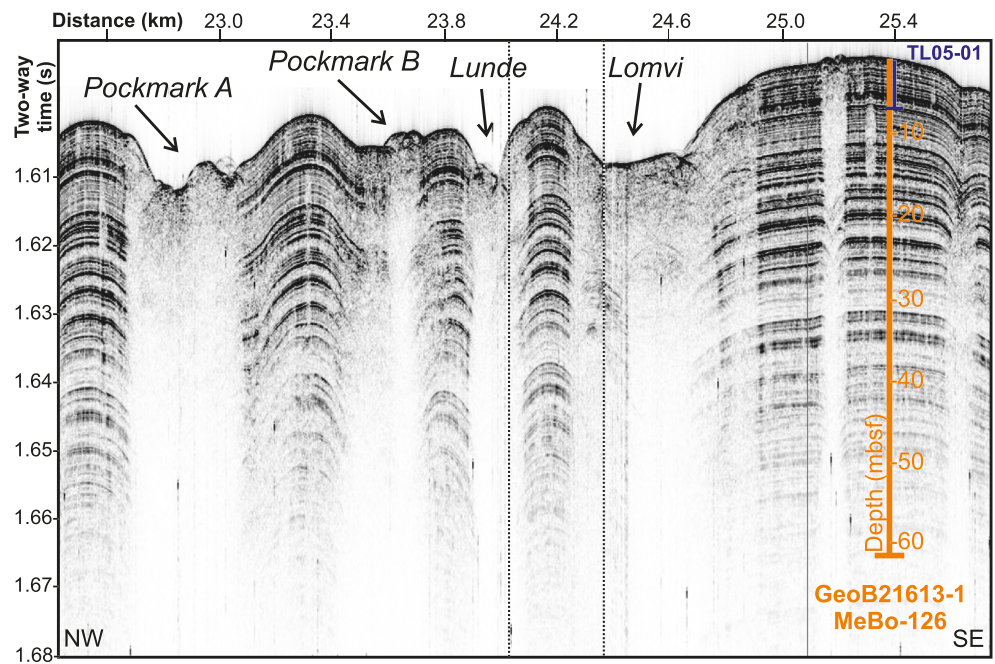
Figure 8. Sections of PARASOUND subbottom profiler data along the crest of the Vestnesa Ridge across the chain of pockmarks (vertical exaggeration: 32). Location of the deep reference borehole with 62 m penetration (GeoB21613-1; MeBo126) is shown together with the reference heat probe station TL05-01.

lack constraints on subsurface thermal conductivity which therefore was held constant at 1.5 Wm^{-1} K^{-1}. Thus, the predicted temperature of 11.6°C (sequence TL-11) and 11.3°C (sequence TL 09) at the BSR depth of ~160 mbsf is associated with a large uncertainty.

4. Discussion

4.1. Pockmarks as Site of Increased Heat Flow

From comparison of MeBo70 and heat probe data gathered at the reference site (GeoB21613-1), we argue that the thermal gradients and heat flow values determined with the heat probe are overall robust and representative of the deeper thermal regime after correcting for topographic effects. The study of heat flow around pockmarks did show that the heat flow is systematically increased at all sites within a pockmark depression. This observation was made at Vestnesa and Svyatogor Ridges. Due to the accurate positioning of the heat probe, the differentiation in stations inside or outside a pockmark (e.g., as shown in Figures 3 and 14) is robust.

A systematic increase in heat flow at pockmarks at Vestnesa was not necessarily expected prior to expedition MSM57 based on previous work by, for example, Vogt, Gardner, Crane, Sundvor, et al. (1999) who observed no difference in heat flow at pockmarks of Vestnesa Ridge relative to the assumed background. Higher heat flow within pockmarks associated with gas hydrate occurrences and sites of active gas venting was seen elsewhere (e.g., Römer et al., 2012; Wei et al., 2015); yet, it is unusual to see an increase in heat flow at all pockmark depressions, given the strong lateral variability in gas venting activity (taken as a proxy for possible advection of warmer fluids) at Vestnesa Ridge and a complete absence of gas venting at Svyatogor Ridge. Overall, heat flow at the crests of Vestnesa and Svyatogor Ridges should be lower than at the flanks due to topographic cooling. This effect is not very obvious from our station data, as measurement sites were made almost exclusively on the crests of the ridges and pockmarks. However, some sites measured on the western and eastern slopes at a distance of ~1 km from the crest of Svyatogor Ridge (TL09-06, TL09-07, TL09-08, and TL11-01) showed elevated heat flow values relative to the nonpockmark locations at the crest itself for unknown reasons.
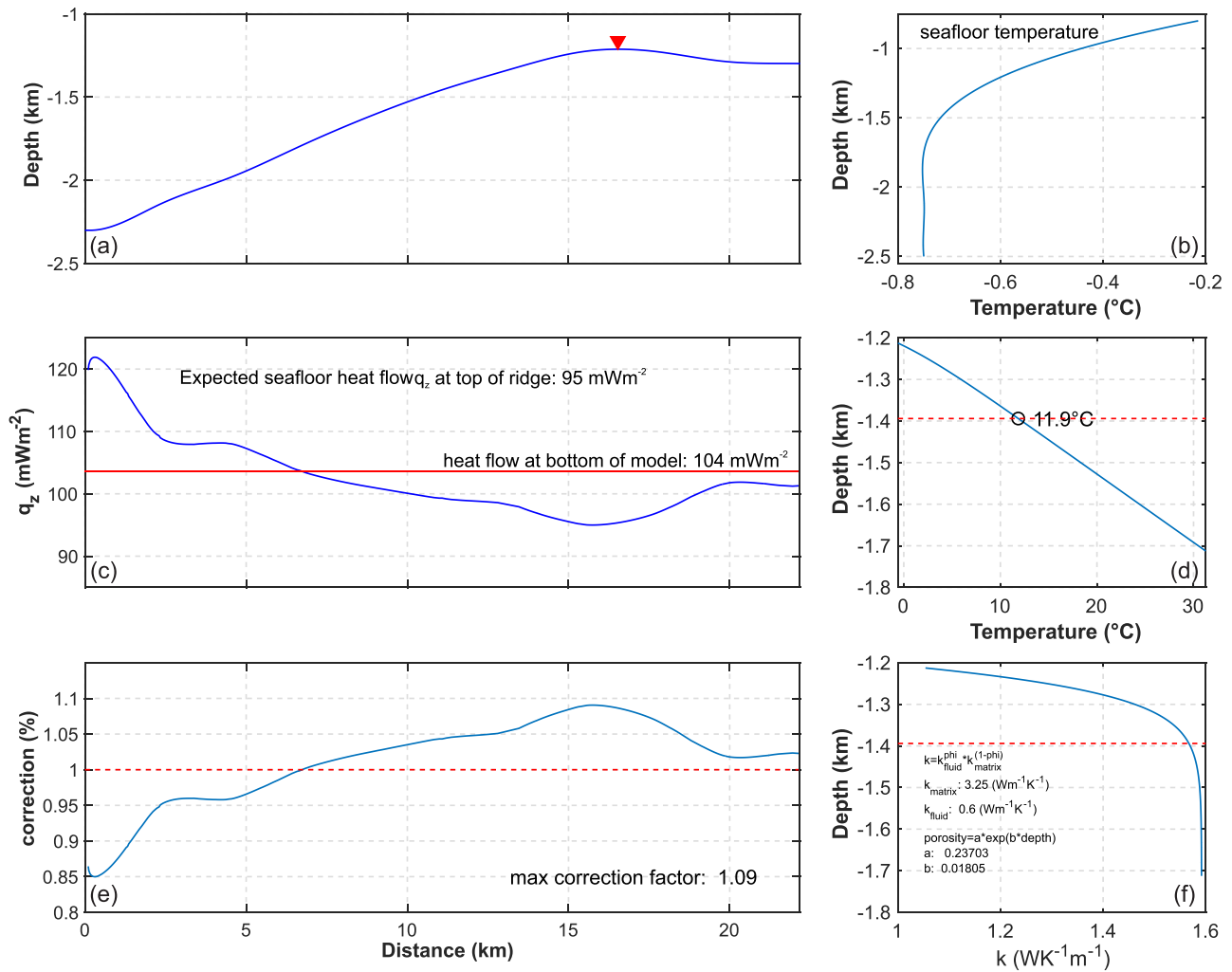
Figure 9. Results of thermal modeling of topographic effect at Vestnesa Ridge on the seafloor heat flow and temperature at depth of BSR (~200 mbsf). The profile is crossing at the reference drill site MeBo126 (GeoB21613-1, red triangle) and semiparallel to the seismic section shown in Figure 7b. Input parameters are (a) topography, (b) seafloor temperature variation as function of water depth, and (f) a depth-dependent thermal conductivity. (c) A background heat flow of ~104 mW m^{-2} is used in order to reproduce the measured heat flux at the reference drill site of ~95 mW m^{-2}. (d) Depth-dependent temperature at the reference site. (e) A maximum topographic correction of 10% is seen for the region of the pockmark chain along the crest of Vestnesa Ridge.

Although heat flow was generally higher inside than outside a pockmark, the dense measurement points at Lunde show also some significant variation within the pockmark itself (Figures 3 and 6). The local variation of heat flow inside Lunde pockmark is in the order of 20 mW m^{-2} (95–115 mW m^{-2}) and values are all higher inside than outside the pockmark. The high variability of heat flow can be attributed to lateral changes in the subseafloor plumbing system. As seen from historical data (Smith et al., 2014), gas venting at the pockmark chain of Vestnesa Ridge was not always seen at the same exact locations. The advection of fluids and gases along faults and fractures allows the formation of gas hydrate, which could then create plugs for further advection of fluids. New pathways are created by fracturing of the sediments due to the fluid/gas pressure from below and new gas venting outlets are created. The seepage at Vestnesa Ridge is suggested to have been active since the last 1.5 Ma (Plaza-Faverola et al., 2015). Seepage is hypothesized to be varying in time and be linked to large-scale tectonic stress regime changes.

Although no gas venting has been seen at pockmarks "A" and "B" and not along the entire Svyatogor Ridge during expedition MSM57, the systematic increase of heat flow inside the pockmarks suggests that these structures are still reflecting anomalous temperature regimes. However, measured temperature profiles inside the pockmarks do not show any indication of advective heat transport (i.e., an absence of a curvature in the temperature values with depth). The absence of such characteristic curvature may be related to the
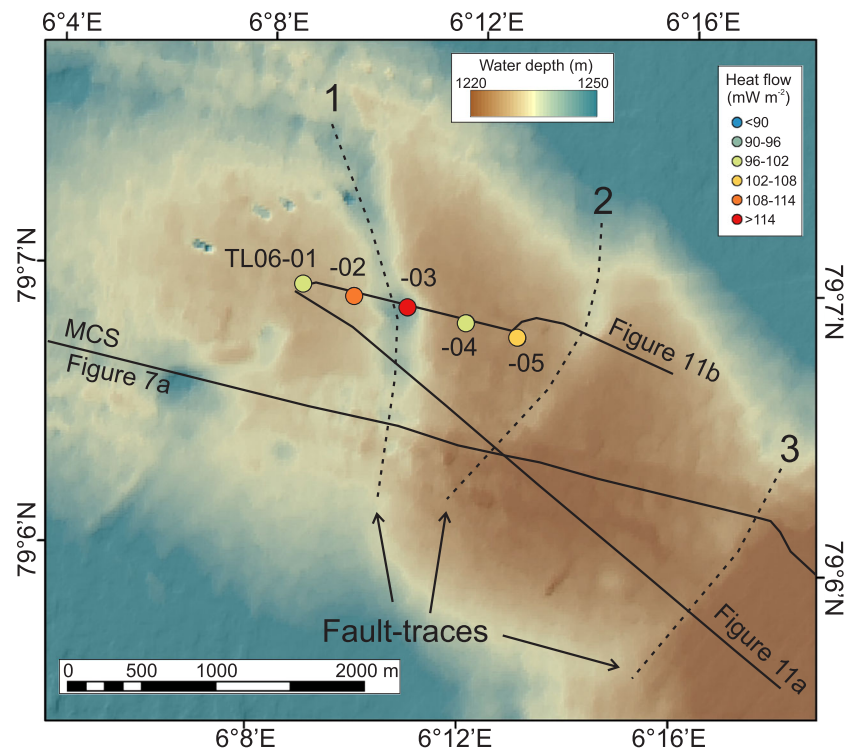
Figure 10. Map showing results of heat flow measurements across northern fault zone. Three fault traces are visible in bathymetry and PARASOUND data (compare to Figure 11). The highest heat flow value of 125 mW m^{-2} is seen inside Fault Trace 1.

maximum penetration depth of ~6 m of the heat probe linked to possibly small upward fluid flow velocities. Alternatively, if strong seasonal changes in bottom temperature exist, they also could alter the curvature of the temperature record with depth to a point of potentially canceling out fluid flow related effects (e.g., Bense & Kooi, 2004). Only long-term observations over several seasonal cycles could help unravel this phenomenon.

4.2. Base of Gas Hydrate Stability and BSR Depth

One of the uncertainties in previous attempts to calibrate the BGHSZ with the seismically observed BSR was an unknown deeper thermal gradient for Vestnesa Ridge (e.g., Plaza-Faverola et al., 2017). Additionally, laterally varying relative amounts of nonmethane hydrocarbons (seen between gravity cores GC10 near the reference site and GC19, Table 1) make the prediction of the BGHSZ more complex. As shown by Plaza-Faverola et al. (2017), a match between BSR and theoretical BGHSZ can be achieved by changing the gas composition and/or thermal gradients. Smith et al. (2014) further modeled the feed-gas composition order to account for molecular fractionation that may happen during hydrate crystallization (e.g., Pape et al., 2010; Sloan, 1998) and to subsequently model the hydrate stability zone to reproduce the gas composition in recovered gas hydrate samples at the Lunde pockmark (gravity core GC929).

However, our measurements of a background thermal gradient of ~78 mK m^{-1} is lower than all constraints previously assumed. With the reduced thermal gradient, the theoretical calculations of the BGHSZ require less light nonmethane hydrocarbons and shift the gas composition closer to a methane-dominated system. As shown by Pape et al. (2020) for Vestnesa Ridge, hydrocarbon gas composition at sites distant to focused fluid migration does not just vary significantly laterally between sites but does also change with depth. Fluid migration of thermogenic gases (relatively enriched in light nonmethane hydrocarbons) is mainly controlled by faults and is thus concentrated toward pockmarks.

The systematically increased thermal gradient and hence heat flow within the pockmarks compared to regions away from pockmarks could be the result of advective heat transport within the pockmarks;
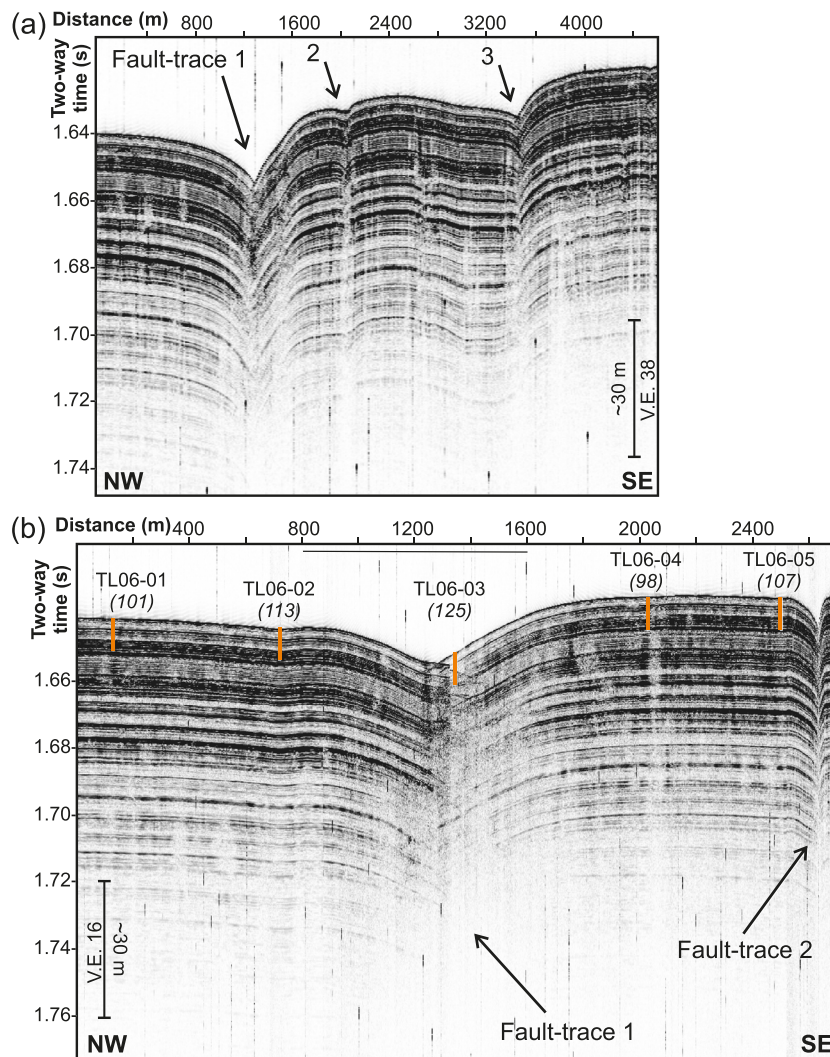
Figure 11. PARASOUND data across the northern fault line region: (a) Segment of the profile connecting all three fault traces seen in this region and (b) segment across the five heat probe stations (orange lines indicate maximum penetration of ~5.7 m). Locations of lines see Figure 10. Heat flow values (in mW m^{-2}) are shown in parentheses at each station location.

however, the linear temperature profiles measured indicate no signs of significant fluid flow. In terms of estimating the depth of the BSR and BGHSZ, the increase in heat flow inside a pockmark is counteracting the effect of advection of thermogenic gases and thus, the BGHSZ may only change slightly underneath pockmarks. This lack of depth variation was already noted by Plaza-Faverola et al. (2017) and attributed to the overall uncertainties in the assumptions used in their analyses.

We have used all available data from thermal measurements, thermal modeling constraints, as well as gas chemistry to investigate the depth of the BGHSZ and BSR (Figure 15). Using all measurements of void gases from regular coring as well as pressure cores up to a depth of 62.5 mbsf (Pape et al., 2020), the limit of the phase boundary for the sample locations (in mbsf) was calculated. The equilibrium conditions with the gas compositions from MeBo drilling suggest gas hydrate structure 1 (sI) is formed. Incorporating the gas composition of GC19 (Plaza-Faverola et al., 2017) yield equilibrium conditions for structure 2 (sII) gas hydrate. Based on these data, we estimated an average sI phase boundary for the Vestnesa Ridge system and extrapolated this boundary to the depth of the assumed BGHSZ. Assuming a linear background thermal gradient intersects the average sI phase boundary at ~205 mbsf. Using the thermal modeling results, a depth
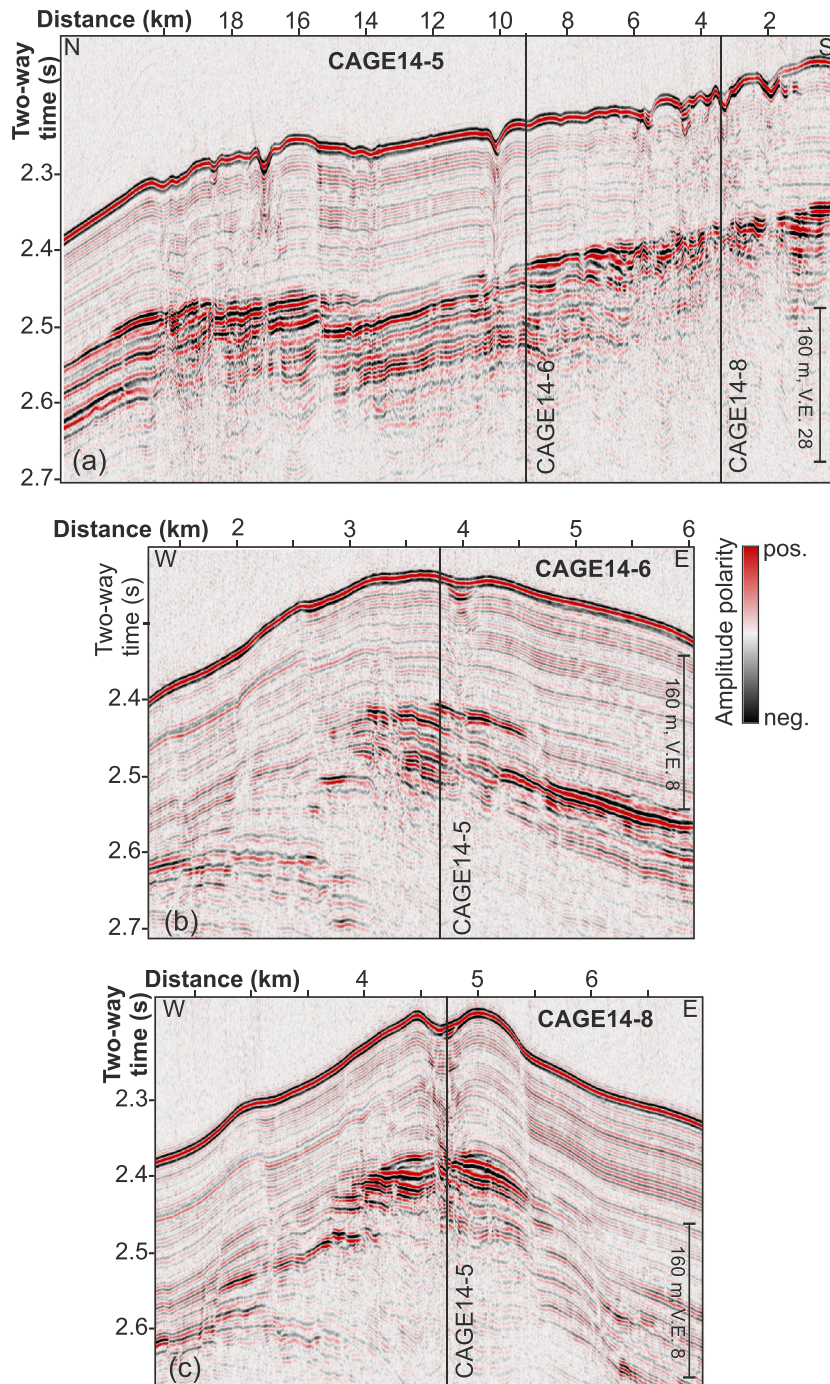
Figure 12. MCS data across Svyatogor Ridge showing BSR as bright amplitude truncation. (a) Line CAGE14-5 along the crest of the ridge, (b) Line CAGE14-6 perpendicular to the ridge and at the deployment series TL11, and (c) Line CAGE14-8 perpendicular to the ridge and at the deployment series TL09. Locations see Figures 1b and 14. Amplitude polarity is identical on all three sections.

of the BGHSZ is seen at ~245 mbsf due to the downward deflection of the temperature profile. Seismically, the BGHSZ is assumed to be imaged by the BSR.

BSR depth was estimated from the seismic data to ~195 mbsf (Plaza-Faverola et al., 2017) with 0.23 s difference in two-way travel time between seafloor and BSR and a velocity of 1,680 m/s. Increasing velocity by 100 m/s shifts the BSR by ~10 m to 205 mbsf. An even higher increase in velocity to 2,100 m/s is required
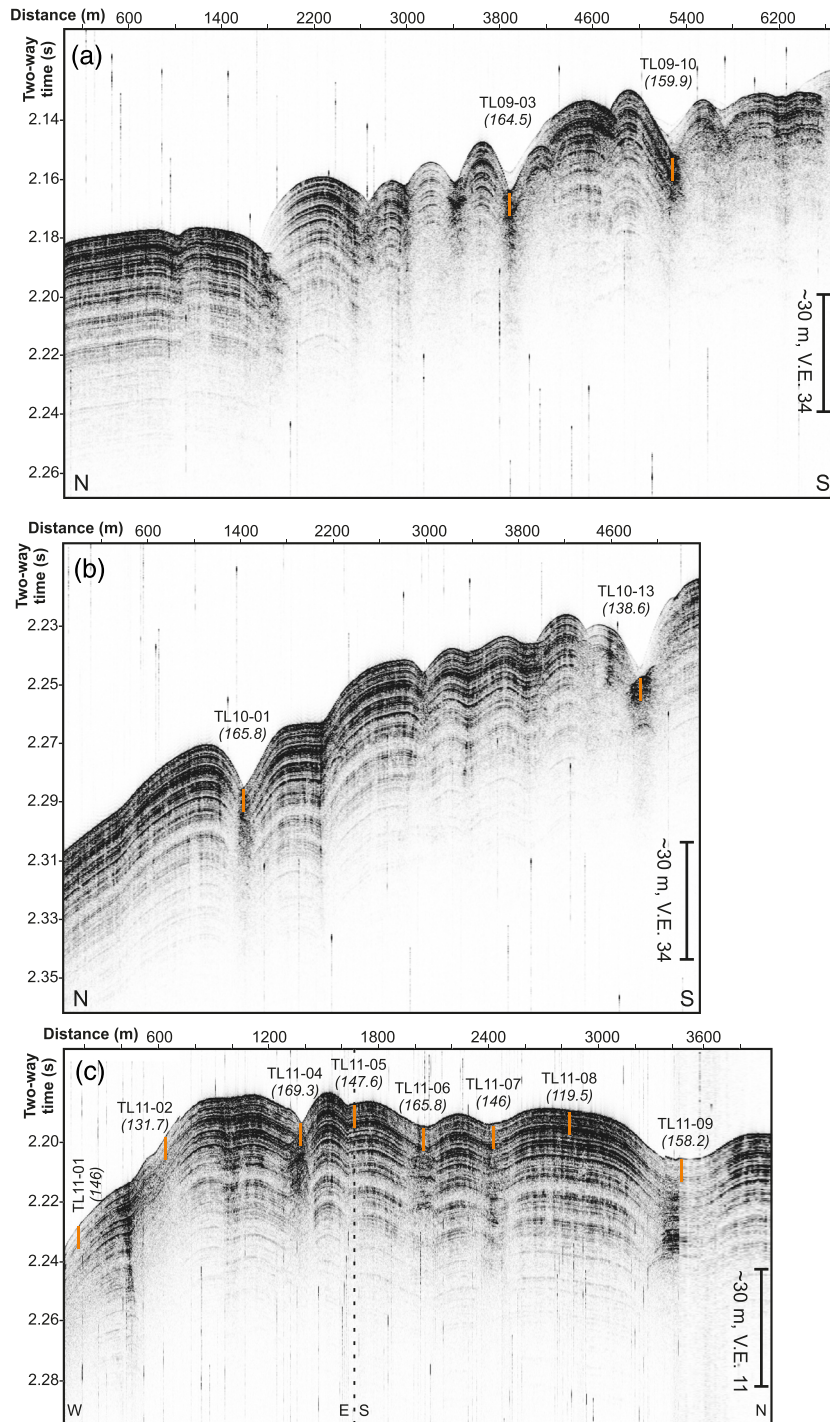
Figure 13. Profiles of PARASOUND subbottom data across the three heat probe transects at Svyatogor Ridge: (a) deployment series TL-09 (southernmost site), (b) deployment series TL-10 (northernmost site), and (c) deployment series TL-11 (central site with L-shape profile). Locations see Figure 14. Heat flow values (in mW m^{-2}) are shown in parentheses at each station location (orange line indicates penetration depth of probe).

to shift the BSR depth to 245 mbsf, the intersection of the sI phase boundary with the temperature profile from 2D thermal modeling. One velocity depth profile at Vestnesa Ridge ~30 km west of the MeBo reference site was derived using reflection seismic travel time modeling of OBS data (Petersen et al., 2010). The velocity gradually increases with depth to a maximum value near 1,700 m/s close to the
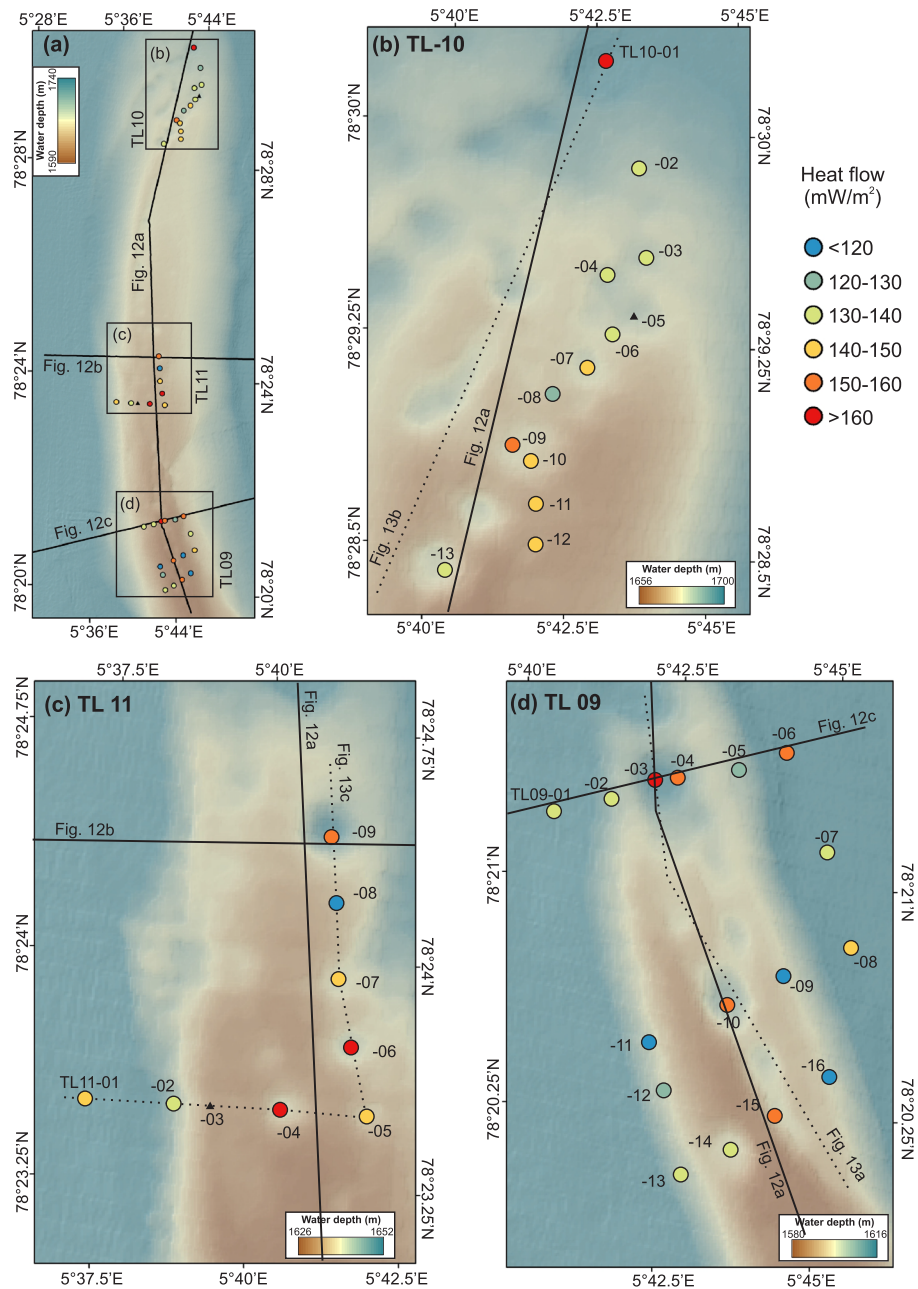
Figure 14. Results of heat probe deployments at Svyatogor Ridge: (a) Overview of the pockmark chains and deployment stations. (b) northern segment with stations of deployment series TL10, (c) central portion of ridge with stations of deployment series TL11, and (d) southern segment with stations of deployment series TL09. Color code of heat flow values (indicates in legend) is identical in all sub plots. Locations of the seismic (Figure 12) and PARASOUND (Figure 13) profiles are shown as solid and dotted lines, respectively.

BSR. A very similar *P* wave velocity depth structure was defined by Goswami et al. (2015) in a profile along line JR211_17 (Figure 7b) across Vestnesa Ridge and the Lunde pockmark using traveltime inversion of reflection data obtained with two OBS instruments. New and more detailed results of the *P* wave velocity structure beneath the crest of Vestnesa Ridge across the pockmark chain were obtained by Singhroha et al. (2019, 2020). In general, the depth profile of velocity is similar to the previous work, but some local anomalies with *P* wave velocities as high as 1900 m/s above the BSR were found. *P* wave velocity anisotropy induced by gas hydrate-bearing faults was also studied (Singhroha et al., 2020) and velocity can be up to 5% higher (~80 m/s) for seismic rays that cross a fault plane perpendicular. However, given
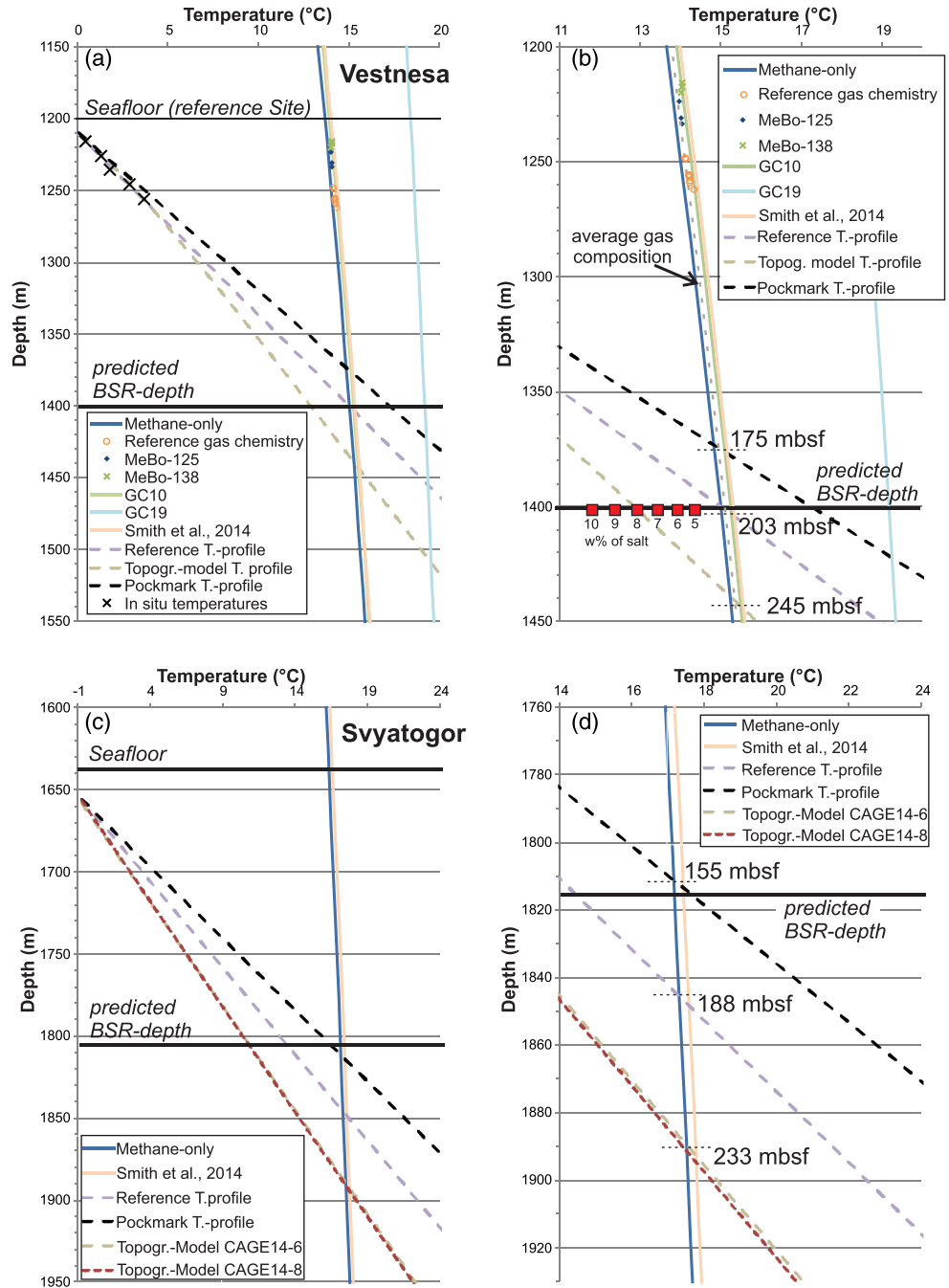
Figure 15. Theoretical gas hydrate phase boundaries for different gas compositions: (a) and (b) Vestnesa Ridge reference site (1,200 m water depth), and (c) and (d) Svyatogor Ridge (1,657 m water depth). A pure methane (CH_4) system (blue line) results in the shallowest base of hydrate stability (sI) for any thermal gradient. Shown are background (dashed purple) and elevated (dashed black) gradients inside pockmarks, as well as from topographic modeling. The BSR at Vestnesa Ridge is at ~200 m below seafloor (mbsf). At Svyatogor Ridge, the BSR is at ~160 mbsf. Increasing pore fluid salinity to ~8 weight percent (wt.%) is required at Vestnesa Ridge to match the base of hydrate stability (sI) with the 2-D topographic model for an assumed average gas mix from MeBo cores at the reference site. Phase boundaries for gas compositions at gravity core GC10 (sI) and GC19 (sII) from Plaza-Faverola et al. (2017) and seafloor feed gas (sI) by Smith et al. (2014) are included.

these studies as well as the general nature of sediments and their depositional character as contourite deposits along and across the ridge makes a drastically higher velocity to deepen the BSR depth from seismic travel time observations rather unrealistic.

In order to match a theoretical sI gas hydrate phase boundary with this reduced temperature at a fixed BSR depth of 200 mbsf requires higher salt concentrations in the pore water. Modeling the effect of excess salt on the gas hydrate phase boundary was made for several pore fluid salinities varying from 5 to 10 wt.% (red squares in Figure 15). A high value of ~8 wt.% (more than twice that of seawater) is needed to match modeled temperature and phase boundary at 200 mbsf. Not only is this high salinity unrealistic, there is no evidence from drilling and coring that salt concentrations do increase with depth at the reference site. There is no process that could produce such high salt concentrations regionally (i.e., not inside the pockmarks with active gas venting and shallow gas hydrate growth) at rates required such that diffusion is not transporting the salt away and equalizing the pore fluid profile back to seawater concentrations. However, increasing salt concentrations with depth (to values of ~600 mM near the BSR) were seen, for example, at the northern Cascadia margin at drill sites U1325 and U1326 where ash to zeolite transformations were invoked to explain the slight systematic increase in salt concentrations with depth (Riedel et al., 2010). Recent gas hydrate formation can also increase pore fluid salinity as documented at cold vent settings, such as Hydrate Ridge (Torres et al., 2004; Tréhu et al., 2003), and subsequently used to explain how free gas can move freely through the gas hydrate stability field (Liu & Flemings, 2006). At one site inside the Lunde pockmark an enrichment in pore fluid salinity to values of 890 mM from salt-exclusion linked to recent gas hydrate formation was seen (Bohrmann et al., 2017). However, this localized event cannot explain the discrepancy seen between the BSR depth and our modeled BGHSZ (W.-L. Hong, personal communication, October 14, 2020).

Combining the observations of thermal gradients at Vestnesa Ridge from MeBo70 drilling, heat probe deployments, gas compositions of void gas collected at the reference site (MeBo126, GeoB21613-1), and thermal modeling results in a remaining discrepancy in theoretical estimates for the base of the gas hydrate stability and seismically observed depth of the BSR. The range in possible depths of the BGHSZ as constrained from gas molecular chemistry and thermal models at the reference site is from 205 to 245 mbsf. Realistic depths of the BSR underneath the ridge crest range from 185 mbsf (low velocity of 1,600 m/s) to 220 mbsf (high velocity of 1,900 m/s).

A similar discrepancy exists for Svyatogor Ridge between the 2-D topographic model and prediction of the BSR depth from seismic data. Here, a gas mix using the values of required feed-gas composition (Table 1) determined by Smith et al. (2014) is used to model the gas hydrate phase boundary, which was adopted from the approach by Johnson et al. (2015). This feed-gas composition results in an equilibrium for sII gas hydrate to be formed due to the high amounts of propane included. No independent gas compositions are available to date from Svyatogor Ridge. The predicted depth of the BSR at the crest of the ridge (~160 mbsf) matches the theoretical base of gas hydrate stability only for the high geothermal gradient seen in pockmarks. The measured background gradient and the 2-D model predict a significantly deeper base of gas hydrate stability.

A possible explanation of these apparent contradictions is that possibly the 2-D topographic effect is overestimated, some unknown pore fluid chemical mixing may happen at greater depth (drilling only reached to ~62 mbsf) without expression at shallow depths, or a combination of these two processes.

Topographic effects were investigated by 2-D modeling only and thus may incompletely capture additional cooling from 3-D effects. True 3-D effects could deepen the BGHSZ as, for example, shown off Taiwan where canyon erosion yielded topographic cooling of exposed ridges (Chen et al., 2014). However, the geometry of Vestnesa Ridge with a dominant east-west water depth change and little topographic variation along the crest (Figure 1) supports our simplification to do 2-D modeling only, especially as the 2-D effect is estimated to be in the order of 10% only. Little variation in water depth in the along-crest direction would result in small additional adjustments and further deepening of the theoretical sI BGHSZ, thus not explaining our discrepancies in field observation and modeling. A different scenario could be that long-period climate-induced bottom water temperature variations and associated sea level changes have impacted the GHSZ. However, for the period since the last glacial maximum, the reduced sea level (120 m lower than today) and reduced bottom water temperature (1°C colder than today) are mutually exclusive (Himmler et al., 2019; Plaza-Faverola et al., 2017).

A mismatch in a top of free gas and BGHSZ due to capillary effects was described by Liu and Flemings (2011). Variations in the pore size distribution can result in the top of free gas (seismically seen as BSR) being significantly shallower (or deeper) than the equilibrium depth of the BGHSZ. The BSR is systematically shallower relative to the BGHSZ (at equilibrium) for greater water depths. Capillary effects inhibit the growth of gas hydrate in narrow pores and thus act like an inhibitor (e.g., salt) to gas hydrate stability (Liu & Flemings, 2011). Smaller pore sizes do promote an upward shift of the free gas occurrences and thus a BSR shallower than predicted by the hydrate stability model.

Due to the lack of deeper core data near the BGHSZ, we cannot definitively rule out any of the above discussed factors as possible reason for the observed discrepancy. New drilling with detailed downhole in situ temperature measurements, collecting gas and pore water geochemical data, performing in situ geophysical logging (measuring P wave velocity), as well as measuring sediment physical properties (density and porosity) including grain size will help narrowing down the uncertainties involved in modeling the BGHSZ.

Although no definitive solution can be presented at this stage, our study highlights the need for a comprehensive data set when attempting to describe the nature of gas hydrate distribution and characterize fluid and gas migration through the GHSZ. Using, for example, the depth of the BSR alone to estimate heat flow is highly uncertain as many assumptions are required in the mathematical derivation, including estimates on the depth-dependent sediment porosity and/or thermal conductivity, P wave velocity, grain size, gas and pore fluid chemical composition, and, last but not least, topographic effects. Our data set from Vestnesa Ridge is also not complete in that regard as we were limited to a maximum penetration depth of ~60 mbsf but newly provides many of these required parameters and thus represents a step forward in our understanding of such gas hydrate occurrences.

5. Conclusion

Drilling at Vestnesa Ridge was completed with the MARUM-MeBo70 seafloor drilling rig and in situ temperature measurements were carried out at selected depths during coring to estimate the thermal gradient. At a reference site outside of pockmarks and sites of active fluid flow, five downhole temperature measurements up to 55.4 mbsf revealed a thermal gradient of ~80°C km^{-1}. Together with an average gas composition defined at the reference drill site the base of gas hydrate stability was determined to be around 200 ($\pm$10) mbsf or up to 245 mbsf depending on the thermal model used. The depth of the seismically observed BSR at 195 ($\pm$20) mbsf is shallower than predictions based on thermal modeling or linear thermal gradients. Possible reasons for the discrepancy are in the considerable uncertainty in defining the physical properties involved, foremost seismic velocity and thermal conductivity, as well as gas compositions near BSR depths, all require deep drilling to below BSR depth. Additionally, capillary effects from the small-grained sediments deposited at Vestnesa and Svyatogor Ridges may promote a shallower occurrence of free gas (which is seen as BSR) than predicted from the phase-equilibrium modeling.

The downhole data are combined with 63 heat probe deployments around pockmarks along the crest of Vestnesa Ridge. The heat probe data show that heat flow is systematically increased by up to 20 mW m^{-2} inside a pockmark relative to the region outside a pockmark, although heat flow varies significantly within a single pockmark itself. The investigation of pockmarks was extended to the Svyatogor Ridge, about 70 km south of Vestnesa Ridge and south of the Molloy Fracture Zone, where multibeam seafloor imaging showed several chains of pockmarks. Heat flow measurements at 37 stations inside and outside of pockmarks showed the same systematic difference of enhanced heat flow inside of pockmarks. At Svyatogor Ridge, the heat flow inside a pockmark is on average 150 mW m^{-2}, whereas heat flow outside the depressions is ~128 mW m^{-2}. Thus, definition of fluid flow activity should not only be based on observations of active gas discharge (acoustically seen in the water column) and include heat flow measurements.

Data Availability Statement

The raw data on in situ temperature and thermal conductivity measurements conducted during expedition MSM57 are available through the Pangaea data repository (https://doi.org/10.1594/PANGAEA.911766; Riedel, 2020). Multibeam EM122 data used to create seafloor bathymetric maps for this study are available at the Pangaea data repository (https://doi.org/10.1594/PANGAEA.895661). All seismic data shown in this study are stored at the CAGE (Centre for Arctic Gas Hydrate) data repository (https://doi.org/10.18710/

OMF3UX) or can be accessed by contacting Stefan Bünz (stefan.buenz@uit.no). Information and data from Expedition JR211 can be found at the British Oceanographic Data Centre (BODC; https://www.bodc.ac.uk/resources/inventories/cruise_inventory/report/9045/).

References

Bense, V., & Kooi, H. (2004). Temporal and spatial variations of shallow subsurface temperature as a record of lateral variations in groundwater flow. *Journal of Geophysical Research*, *109*, B04103. https://doi.org/10.1029/2003JB002782

Berndt, C., Feseker, T., Treude, T., Krastel, S., Liebetrau, V., Niemann, H., et al. (2014). Temporal constraints on hydrate-controlled methane seepage off Svalbard. *Science*, *343*(6168), 284–287. https://doi.org/10.1126/science.1246298

Bohrmann, G., Ahrlich, F., Bergenthal, M., Bünz, S., Düßmann, R., Ferreira, C., et al. (2017). R/V MARIA S. MERIAN Cruise report MSM57, gas hydrate dynamics at the continental margin of Svalbard, Reykjavik–Longyearbyen–Reykjavik, 29 July–07 September 2016. Berichte, MARUM-Zentrum für Marine Umweltwissenschaften, Fachbereich Geowissenschaften, Universität Bremen, No. 314, 204 pp, Bremen, 2017. ISSN 2195-7894. Retrieved from http://nbn-resolving.de/urn:nbn:de:gbv:46-00105895-15

Bünz, S., Polyanov, S., Vadakkepuliyambatta, S., Consolaro, C., & Mienert, J. (2012). Active gas venting through hydrate-bearing sediments on the Vestnesa Ridge, offshore W-Svalbard. *Marine Geology*, *332–334*, 189–197. https://doi.org/10.1016/j.margeo.2012.09.012

Chen, L., Chi, W.-C., Wu, S.-K., Liu, C.-S., Shyu, C.-T., Wang, Y., & Lu, C.-Y. (2014). Two dimensional fluid flow models at two gas hydrate sites offshore southwestern Taiwan. *Journal of Asian Earth Sciences*, *92*, 245–253. https://doi.org/10.1016/j.jseaes.2014.01.004

Crane, K., Sundvor, E., Buck, R., & Martinez, F. (1991). Rifting in the northern Norwegian-Greeland Sea: Thermal tests of asymmetric spreading. *Journal of Geophysical Research*, *96*(B9), 14,529–14,550. https://doi.org/10.1029/91JB01231

Ferré, B., Jansson, P. G., Moser, M., Serov, P., Portnov, A., Graves, C. A., et al. (2020). Reduced methane seepage from Arctic sediments during cold bottom-water conditions. *Nature Geoscience*, *13*(2), 144–148. https://doi.org/10.1038/s41561-019-0515-3

Freudenthal, T., & Wefer, G. (2013). Drilling cores on the sea floor with the remote-controlled sea floor drilling rig MeBo. *Geoscientific Instrumentation, Methods and Data Systems*, *2*(2), 329–337. https://doi.org/10.5194/gi-2-329-2013

Goswami, B. K., Weitemeyer, K. A., Minshull, T. A., Sinha, M. C., Westbrook, G. K., Chabert, A., et al. (2015). A joint electromagnetic and seismic study of an active pockmark within the hydrate stability field at the Vestnesa Ridge, west Svalbard margin. *Journal of Geophysical Research: Solid Earth*, *120*, 6797–6822. https://doi.org/10.1002/2015JB012344

Grevemeyer, I., & Villinger, H. (2001). Gas hydrate stability and the assessment of heat flow through continental margins. *Geophysical Journal International*, *145*(3), 647–660. https://doi.org/10.1046/j.0956-540x.2001.01404.x

Himmler, T., Sahy, D., Martma, T., Bohrmann, G., Plaza-Faverola, A., Bünz, S., et al. (2019). A 160,000-year-old history of tectonically controlled methane seepage in the Arctic. *Science Advances*, *5*, eaaw1450. https://doi.org/10.1126/sciadv.aaw1450

Hustoft, S., Bünz, S., Mienert, J., & Chand, S. (2009). Gas hydrate reservoir and active methane-venting province in sediments on <20 Ma young oceanic crust in the Fram Strait, offshore NW-Svalbard. *Earth and Planetary Science Letters*, *284*(1–2), 12–24. https://doi.org/10.1016/j.epsl.2009.03.038

Hyndman, R. D., Davis, E. E., & Wright, J. A. (1979). The measurement of marine geothermal heat flow by a multi-penetration probe with digital acoustic telemetry and in situ thermal conductivity. *Marine Geophysical Researches*, *4*(2), 181–205. https://doi.org/10.1007/BF00286404

Johnson, J. E., Mienert, J., Plaza-Faverola, A., Vadakkepuliyambatta, S., Knies, J., Bünz, S., et al. (2015). Abiotic methane from ultraslow-spreading ridges can charge Arctic gas hydrates. *Geology*, *43*(5), 371–374. https://doi.org/10.1130/G36440.1

Kopf, A., Asshoff, K., Belke-Brea, M., Bergenthal, M., Bohrmann, G., Brüunig, A., et al. (2012). Report and preliminary results of R/V SONNE cruise SO222. MEMO: MeBo drilling and in situ Long-term Monitoring in the Nankai Trough accretionary complex, Japan. Leg A: Hong Kong, PR China, 09.06.2012 - Nagoya, Japan, 30.06.2012. Leg B: Nagoya, Japan, 04.07.2012 - Pusan, Korea, 18.07.2012. Berichte, MARUM - Zentrum für Marine Umweltwissenschaften, Fachbereich Geowissenschaften, Universität Bremen, No. 297, 121 pp, Bremen, 2013. ISSN 2195-9633. Retrieved from https://media.suub.uni-bremen.de/handle/elib/3013

Lister, C. R. B. (1979). The pulse-probe method of conductivity measurement. *Geophysical Journal International*, *57*(2), 451–461. https://doi.org/10.1111/j.1365-246X.1979.tb04788.x

Liu, X., & Flemings, P. B. (2006). Passing gas through the hydrate stability zone at southern Hydrate Ridge, offshore Oregon. *Earth and Planetary Science Letters*, *241*(1–2), 211–226. https://doi.org/10.1016/j.epsl.2005.10.026

Liu, X., & Flemings, P. B. (2011). Capillary effects on hydrate stability in marine sediments. *Journal of Geophysical Research*, *116*, B07102. https://doi.org/10.1029/2010JB008143

Panieri, G., Bünz, S., Fornari, D. J., Escartin, J., Serov, P., Jansson, P., et al. (2017). An integrated view of the methane system in the pockmarks at Vestnesa ridge, 79°N. *Marine Geology*, *390*, 282–300. https://doi.org/10.1016/j.margeo.2017.06.006

Panieri, G., James, R. H., Camerlenghi, A., Westbrook, G. K., Consolaro, C., Cacho, I., et al. (2014). Record of methane emissions from the West Svalbard continental margin during the last 23.500 yrs revealed by δ^{13}C of benthic foraminifera. *Global and Planetary Change*, *122*, 151–160. https://doi.org/10.1016/j.gloplacha.2014.08.014

Pape, T., Bahr, A., Rethemeyer, J., Kessler, J. D., Sahling, H., Hinrichs, K. U., et al. (2010). Molecular and isotopic partitioning of low-molecular weight hydrocarbons during migration and gas hydrate precipitation in deposits of a high-flux seepage site. *Chemical Geology*, *269*(3–4), 350–363. https://doi.org/10.1016/j.chemgeo.2009.10.009

Pape, T., Bünz, S., Hong, W.-L., Torres, M., Riedel, M., Panieri, G., et al. (2020). Origin and transformation of light hydrocarbons ascending at an active pockmark on Vestnesa Ridge, Arctic Ocean. *Journal of Geophysical Research: Solid Earth*, *125*, e2018JB016679. https://doi.org/10.1029/2018JB016679

Petersen, C. J., Bünz, S., Huston, S., Mienert, J., & Klaeschen, D. (2010). High-resolution P-Cable 3D seismic imaging of gas chimney structures in gas hydrated sediments of an Arctic sediment drift. *Marine and Petroleum Geology*, *27*(9), 1981–1994. https://doi.org/10.1016/j.marpetgeo.2010.06.006

Pfender, M., & Villinger, H. (2002). Miniaturized data loggers for deep sea sediment temperature gradient measurements. *Marine Geology*, *186*(3–4), 557–570. https://doi.org/10.1016/S0025-3227(02)00213-X

Plaza-Faverola, A., Bünz, S., Johnson, J. E., Chand, S., Knies, J., Mienert, J., & Franek, P. (2015). Role of tectonic stress in seepage evolution along the gas hydrate charged Vestnesa Ridge, Fram Strait. *Geophysical Research Letters*, *42*, 733–742. https://doi.org/10.1002/2014GL062474

Plaza-Faverola, A., Vadakkepuliyambatta, S., Hong, W.-L., Mienert, J., Bünz, S., Chand, S., & Greinert, J. (2017). Bottom-simulating reflector dynamics at the Arctic thermogenic gas provinces: An example from Vestnesa Ridge, offshore west Svalbard. *Journal of Geophysical Research: Solid Earth*, *122*, 4089–4105. https://doi.org/10.1002/2016JB013761

Posewang, J., & Mienert, J. (1999). High-resolution seismic studies of gas hydrates west of Svalbard. *Geo-Marine Letters*, *19*(1–2), 150–156. https://doi.org/10.1007/s003670050102

Riedel, M. (2020). In situ sediment temperature and sediment thermal conductivity measurements with heat flow probe during Maria S. Merian cruise MSM57, PANGAEA, https://doi.org/10.1594/PANGAEA.911766

Riedel, M., Collett, T. S., & Malone, M. (2010). Expedition 311 synthesis: Scientific findings. In Riedel, M., Collett, T. S., Malone, M. J., and the Expedition 311 Scientists, Proc. IODP, 311: Washington, DC (Integrated Ocean Drilling Program Management International, Inc.). https://doi.org/10.2204/iodp.proc.311.213.2010

Riedel, M., Wallmann, K., Berndt, C., Pape, T., Freudenthal, T., Bergenthal, M., et al. (2018). In situ temperature measurements at the Svalbard continental margin: Implications for gas hydrate dynamics. *Geochemistry, Geophysics, Geosystems*, *19*, 1165–1177. https://doi.org/10.1002/2017GC007288

Römer, M., Sahling, H., Pape, T., Bahr, A., Feseker, T., Wintersteller, P., & Bohrmann, G. (2012). Geological control and magnitude of methane ebullition from a high-flux seep area in the Black Sea—The Kerch seep area. *Marine Geology*, *319–322*, 57–74. https://doi.org/10.1016/j.margeo.2012.07.005

Singhroha, S., Bünz, S., Plaza-Faverola, A., & Chand, S. (2020). Detection of gas hydrates in faults using azimuthal seismic velocity analysis, Vestnesa Ridge, W-Svalbard Margin. *Journal of Geophysical Research: Solid Earth*, *125*, e2019JB017949. https://doi.org/10.1029/2019JB017949

Singhroha, S., Chand, S., & Bünz, S. (2019). Constraints on gas hydrate distribution and morphology in Vestnesa Ridge, western Svalbard margin, using multicomponent ocean-bottom seismic data. *Journal of Geophysical Research: Solid Earth*, *124*, 4343–4364. https://doi.org/10.1029/2018JB016574

Sloan, E. D. (1998). *Clathrate hydrates of natural gas*. New York: Marcel Dekker.

Smith, A. J., Mienert, J., Bünz, S., & Greinert, J. (2014). Thermogenic methane injection via bubble transport into the upper Arctic Ocean from the hydrate-charged Vestnesa Ridge, Svalbard. *Geochemistry, Geophysics, Geosystems*, *15*, 1945–1959. https://doi.org/10.1002/2013GC005179

Torres, M. E., Wallmann, K., Tréhu, A. M., Bohrmann, G., Borowski, W. S., & Tomaru, H. (2004). Gas hydrate growth, methane transport, and chloride enrichment at the southern summit of Hydrate Ridge, Cascadia margin off Oregon. *Earth and Planetary Science Letters*, *226*(1–2), 225–241. https://doi.org/10.1016/j.epsl.2004.07.029

Tréhu, A. M., Bohrmann, G., Rack, F., & Torres, M. E. (2003). Proc. ODP, Init. Repts. 204 [Online]. http://ww-odp.tamu.edu/publications/204_IR/204ir.htm

Vanneste, M., Guidard, S., & Mienert, J. (2005). Bottom-simulating reflections and geothermal gradients across the western Svalbard margin. *Terra Nova*, *17*(6), 510–516. https://doi.org/10.1111/j.1365-3121.2005.00643.x

Villinger, H., & Davis, E. E. (1986). A new reduction algorithm for marine heat flow measurements. *Journal of Geophysical Research*, *92*(B12), 12,846–12,856. https://doi.org/10.1029/JB092iB12p12846

Villinger, H. W., Tréhu, A. M., & Grevemeyer, I. (2010). Seafloor marine heat flux measurements and estimation of heat flux from seismic observations of bottom simulating reflectors. In M. Riedel, E. C. Willoughby, S. Chopra (Eds.), *Geo-physical characterization of gas hydrates* (pp. 279–300). Tulsa, OK: Society of Exploration Geophysicists.

Vogt, P. R., Crane, K., Sundvor, E., Max, M. D., & Pfirman, S. L. (1994). Methane-generated(?) pockmarks on young, thickly sedimented oceanic-crust in the Arctic - Vestnesa-Ridge, Fram Strait. *Geology*, *22*(3), 255–258. https://doi.org/10.1130/0091-7613(1994)022<0255:MGPOYT>2.3.CO;2

Vogt, P. R., Gardner, J., Crane, K., Sundvor, E., Bowles, F., & Cherkahev, G. (1999). Ground-truthing 11- to 12-kHz side-scan sonar imagery in the Norwegia-Greenland Sea: Part I: Pockmarks on the Vestnesa Ridge and Storegga slide margin. *Geo-Marine Letters*, *19*(1–2), 97–110. https://doi.org/10.1007/s003670050098

Vogt, P. R., Gardner, L., & Crane, K. (1999). The Norwegian-Barents-Svalbard (NBS) continental margin: Introducing a natural laboratory of mass wasting, hydrates, and ascent of sediment, pore water, and methane. *Geo-Marine Letters*, *19*(1–2), 2–21. https://doi.org/10.1007/s003670050088

Vorren, T. O., Laberg, J. S., Blaume, F., Dowdeswell, J. A., Kenyon, N. H., Mienert, J., et al. (1998). The Norwegian Greenland Sea continental margins: Morphology and late Quaternary sedimentary processes and environment. *Quaternary Science Reviews*, *17*(1–3), 273–302. https://doi.org/10.1016/S0277-3791(97)00072-3

Waghorn, K. A., Bünz, S., Plaza-Faverola, A., & Johnson, J. E. (2018). 3-D seismic investigation of a gas hydrate and fluid flow system on an active mid-ocean ridge; Svyatogor Ridge, Fram Strait. *Geochemistry, Geophysics, Geosystems*, *19*, 2325–2341. https://doi.org/10.1029/2018GC007482

Wallmann, K., Riedel, M., Hong, W.-L., Patton, H., Hubbart, A., Pape, T., et al. (2018). Gas hydrate dissociation at the continental margin off Svalbard induced by isostatic rebound rather than global warming. *Nature Communications*, *9*(1), 83. https://doi.org/10.1038/s41467-017-02550-9

Wei, J., Pape, T., Sultan, N., Colliat, J.-L., Himmler, T., Ruffine, L., et al. (2015). Gas hydrate distributions in sediments of pockmarks from the Nigerian margin—Results and interpretation from shallow drilling. *Marine and Petroleum Geology*, *59*, 359–370. https://doi.org/10.1016/j.marpetgeo.2014.09.013

Westbrook, G., Chand, S., Rossi, G., Long, C., Bünz, S., Camerlenghi, A., et al. (2008). Estimation of gas hydrate concentration from multi-component seismic data at sites on the continental margins of NW Svalbard and the Storegga region of Norway. *Marine and Petroleum Geology*, *25*(8), 744–758. https://doi.org/10.1016/j.marpetgeo.2008.02.003

Westbrook, G., & James Clark Ross cruise 211 scientific party. (2009). Report on Cruise JR211 of RRS James Clark Ross, University of Birmingham, p. 45. Available online at: https://www.bodc.ac.uk/resources/inventories/cruise_inventory/report/9045/

Westbrook, G. K., Thatcher, K. E., Rohling, E. J., Piotrowski, A. M., Pälike, H., Osborne, A. H., et al. (2009). Escape of methane gas from the seabed along the West Spitsbergen continental margin. *Geophysical Research Letters*, *36*, L15608. https://doi.org/10.1029/2009GL039191

Yang, L., Zhao, J., Wang, B., Liu, W., Yang, M., & Song, Y. (2016). Effective thermal conductivity of methane hydrate-bearing sediments: Experiments and correlations. *Fuel*, *179*, 87–96. https://doi.org/10.1016/j.fuel.2016.03.075